Investigation on Frequency Diversity Effects for Various Transmission Schemes Using Frequency Domain Equalizer in DFT-Precoded OFDMA

Lianjun Deng[†], Teruo Kawamura[††], Hidekazu Taoka[†††], and Mamoru Sawahashi[†]

[†] Department of Information Network Engineering, Tokyo City University
[††] Radio Access Network Development Department, NTT DOCOMO, INC.
[†††] DOCOMO Communications Laboratories Europe GmbH

Abstract **-** This paper presents frequency diversity effects of localized transmission, clustered transmission, and intra-subframe frequency hopping (FH) for Discrete Fourier Transform (DFT)-precoded Orthogonal Frequency Division Multiple Access (OFDMA) using a frequency domain equalizer (FDE). In the evaluations, we employ the normalized frequency mean square covariance (NFMSV) as a measure of the frequency diversity effect, i.e., randomization level of the frequency domain interleaving associated with turbo coding. Link-level computer simulation results show that frequency diversity is very effective in decreasing the required average received signal-to-noise power ratio (SNR) at the target average block error rate (BLER) according to the increase in the entire frequency region in DFT-precoded OFDMA using a linear minimum mean square error (LMMSE) based FDE. Moreover, we show that the NFMSV is an accurate measure of the frequency diversity effect for localized transmission in terms of the average BLER and that the NFMSV for the entire frequency region well approximates the frequency diversity effect for clustered transmission. Finally, we show that the effect of intra-subframe FH is saturated at a relatively narrow FH separation and that there is no close relationship between the FH separation and the NFMSV for the intra-subframe FH.

Keywords *- mobile communications; single-carrier FDMA; frequency diversity; frequency domain equalizer; frequency mean square covariance*

I. INTRODUCTION

Single-carrier frequency division multiple access (SC-FDMA) scheme achieves a lower peak-to-average power ratio (PAPR) feature than multicarrier based radio access including orthogonal frequency division multiplexing (OFDM). Hence, SC-FDMA was adopted in the Release 8 Long-Term Evolution (LTE) (Rel. 8 hereafter) uplink for its prioritization of wide area coverage provisioning due to a reduction in the transmission back-off in the transmitter power amplifier [1]. Discrete Fourier transform (DFT)-precoded OFDMA (also called DFT-spread OFDMA) was adopted, which generates SC-FDMA signals in the frequency domain [2], [3] to achieve high commonality with OFDM in the Rel. 8 LTE downlink and affinity to frequency domain equalizers (FDEs) [4], [5].

In the LTE, the maximum transmission bandwidth is 20 MHz. Moreover, in LTE-Advanced, the concept of carrier aggregation was proposed to generate a transmission bandwidth wider than 20 MHz [6]. The main reason for adopting the carrier aggregation concept is to generate a wider transmission bandwidth up to approximately 100 MHz, while maintaining backward compatibility with the LTE user equipment (UE) and eNode B. In such wider transmission bandwidths, frequency diversity, i.e., randomization of the received signal level suffering from frequency-selective fading, aids in mitigating burst errors. This is also true in DFT-precoded OFDMA using a FDE. When powerful channel coding such as turbo coding is employed, the average block error rate (BLER) performance level is worse by approximately two orders of magnitude compared to that at the decoder output. Hence, the impact of the background noise is large in such a poor BLER region. Some key techniques that utilize frequency diversity effects are wideband transmission, frequency domain channel-dependent scheduling, and frequency hopping (FH). In frequency domain channel-dependent scheduling, resource units called resource blocks (RBs) with a high received signal level are assigned to each user at every time slot. Meanwhile, control signals including channel quality indicator (CQI) feedback and resource assignment are necessary. Wideband transmission and FH directly takes advantage of the randomization of fluctuations in the received signal level due to frequency-selective fading. In addition, they do not need associated control signals. In the paper, we focus on wideband transmission and FH in a multipath fading channel with zero specular components, in which each path suffers from independent Rayleigh fading. Hence, we assume complex Gaussian wide-sense stationary uncorrelated scattering (WSSUS) channels [7]. Complex Gaussian WSSUS channels are specified by their scattering functions. Focusing on frequency selectivity, beneficial measures such as the root mean square (r.m.s.) delay spread are often used [7]-[9]. The r.m.s. delay spread of a channel is defined as the variance in the time delay with the normalized delay power profile of the channel as the probability density function. However, it was shown that a close relationship does not exist between the r.m.s. delay spread and the system performance when the channel bandwidth is sufficiently wide. The coherence bandwidth is a more direct measure of the frequency selectivity. The coherence bandwidth with level κ is defined as the widest bandwidth in which the correlation of the channel frequency response is greater than κ, where κ is selected to be close to one between zero and one. Hence, the coherence bandwidth means the bandwidth over which the channel frequency response is highly correlated. The coherence bandwidth is represented using the r.m.s. delay spread as $B_c = 1/h\tau_{rms}$, where h is a constant value [7]-[9]. The relation is often used for instance to measure the effect of channel coding associated with frequency domain interleaving. However, it was shown in [10] and [11] that there is no close relationship between the coherent bandwidth and system performance when the channel bandwidth is wide relative to the coherence bandwidth. Hence, a more accurate measure for frequency selectivity called the normalized frequency mean square covariance (NFMSV) was proposed [10],[11]. The NFMSV is the absolute-squared auto-covariance of the frequency response averaged over all considered frequency regions. In [10] and [11], it was shown that the NFMSV provides a very close relationship to the bit error rate (BER) using the Reed-Solomon code or convolutional code for FH spread spectrum (FHSS) and direct sequence spread spectrum (DSSS) systems.

In the paper, we present the frequency diversity effects of localized transmission, clustered transmission, and intra-subframe

FH for DFT-precoded OFDMA using a FDE. We employ the NFMSV as a measure of the frequency diversity effect, i.e., randomization level of the frequency domain interleaving associated with turbo coding. The performance evaluations in the paper differ from those in [10] and [11] from the following viewpoints. First, [10] and [11] focused on the close relationship between the NFMSV and the average BER. Here, we focus on the frequency diversity effect, i.e., interleaving effect associated with turbo coding for a variable transmission bandwidth in SC-FDMA. Second, in [10] and [11], FHSS and DSSS using a serial interference canceler (SIC) were employed both assuming ideal channel estimation. We assume DFT-precoded OFDMA using a linear minimum mean square error (LMMSE) based FDE. We employ reference signal (RS) based channel estimation (CE) as well. Third, we investigate the frequency diversity effect for various transmission schemes for DFT-precoded OFDMA including localized transmission, clustered transmission, and intra-subframe FH. Note that intra-subframe FH is realistic considering actual channel estimation unlike for FHSS. The rest of the paper is organized as follows. Section II briefly explains the NFMSV as a measure of the frequency diversity effect in the frequency region of interest used in the paper. After describing the computer simulation configuration in Section III, Section IV presents the simulation results followed by the conclusion in Section V.

II. Measure for Frequency Diversity Effect

As aforementioned, we use the NFMSV as a measure for the frequency diversity effect. The NFMSV in the frequency region from A Hz to B Hz is decided as [10], [11]

$$\mu_F = \frac{\int_A^B df \int_A^B df' \left| E\left[H(f)H^*(f')\right]\right|^2}{(B-A)\int_A^B df \left| E\left[H(f)H^*(f)\right]\right|^2} \quad . \quad (1)$$

In (1), $H(f)$ represents a complex frequency response of the channel at frequency f and * denotes a complex conjugate. Since we assume a WSSUS channel, impulse response $h(\tau)$ satisfies $E\left[h(\tau)h^*(\tau')\right] = p(\tau)\delta(\tau-\tau')$, where $p(\tau)$ denotes the complex delay profile of the channel. In this case, it was provided in [10] that the NFMSV, μ_F, is given as

$$\mu_F = \frac{\int_{-\infty}^{\infty} d\tau \int_{-\infty}^{\infty} d\tau' \, p(\tau)p(\tau')\left[\mathrm{sinc}\{\pi(B-A)(\tau-\tau')\}\right]^2}{\left[\int_{-\infty}^{\infty} d\tau p(\tau)\right]^2} \quad . \quad (2)$$

Here, $\mathrm{sinc}(x) = \sin(x)/x$. In the paper, we assume a discrete time channel in which the N-path delay profile is given as $p(\tau) = \sum_{i=1}^{N} p_i \delta(\tau - \tau_i)$. The NFMSV is represented as [10]

$$\mu_F = \frac{\sum_{i=1}^{N}\sum_{j=1}^{N} p_i p_j \left[\mathrm{sinc}\{\pi(B-A)(\tau_i-\tau_j)\}\right]^2}{\left[\sum_{i=1}^{N} p_i\right]^2} \quad . \quad (3)$$

The NFMSV is the absolute-squared auto-covariance of the frequency response, which is averaged over all the frequency regions of interest. Hence, it represents the overall covariance of the channel unlike the coherence bandwidth [11]. We computed the NFMSV values based on (3). We assume 4 types of power delay profile models with N = 9 and 6: the GSM 6-path Typical Urban (TU) channel model with the r.m.s. delay spread of τ_{rms} = 1.06 μs [12]; the ITU 6-path Vehicular-A (VA) with τ_{rms} = 0.38 μs [13]; the 9-path Extended Typical Urban (ETU) channel model with τ_{rms} = 0.99 μs [14]; and the Extended Vehicular-A (EVA) channel model with τ_{rms} = 0.36 μs [14]. We assume that each path follows independent Rayleigh fading.

III. Computer Simulation Configuration

Fig. 1 shows the frame structure assumed in the paper, which is based on that in Rel. 8 LTE [1]. One subframe with a length of 1 ms comprises 14 fast Fourier transform (FFT) blocks, which correspond to the SC-FDMA symbols. Moreover, 1 FFT block contains a 66.7-μs effective data block and 4.7-μs cyclic prefix (CP). The corresponding subcarrier spacing becomes 15 kHz. Since the subframe length is very short, the interleaving effect in the time domain is not obtained. The RS symbols used for channel estimation of coherent detection are multiplexed with the data symbols using time division multiplexing (TDM) into the 4th and 11th FFT blocks. One RB comprises 12 subcarriers (= 180 kHz) in the frequency domain and one subframe in the time domain.

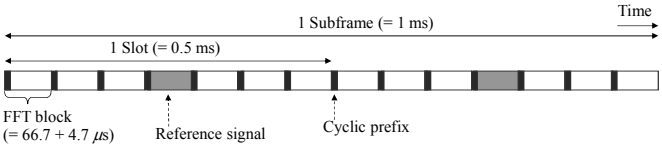

Figure 1. Subframe structure.

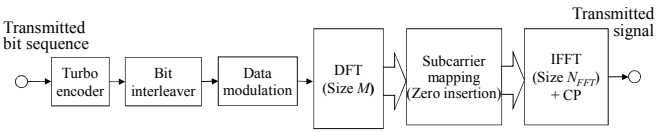

Figure 2. Block diagram of transmitter for DFT-precoded OFDMA.

Fig. 2 shows a block diagram of the transmitter for DFT-precoded OFDMA. The information bit is channel-encoded using a turbo code with the coding rate of R = 1/3 and with the constraint length of K = 4 bits. The generator polynomials are given as $\boldsymbol{G}_{1/3}$ = (1, $\boldsymbol{g}_b/\boldsymbol{g}_a$) and ($\boldsymbol{g}_b/\boldsymbol{g}_a$) where $\boldsymbol{g}_a$ = [1011] and $\boldsymbol{g}_b$ = [1101] [15]. A random interleaver is employed as a turbo interleaver. The bit-interleaver within the duration of one subframe is applied as a channel interleaver. The coded bit sequence is QPSK- or 16QAM-modulated. Let $x_k^{(i)}$ be a data-modulated symbol of the i-th FFT block ($0 \le i \le 13$) for the k-th data-modulated symbol (k = 0,…, M-1), where M denotes the DFT size, which corresponds to the number of subcarriers within the UE transmission bandwidth, B_{Tx}. Note that the modulation phase is known at the receiver for the RS symbols for i = 3 and 10. The i-th FFT block is expressed as $\mathbf{x}^{(i)} = \left[x_0^{(i)}, x_1^{(i)}, \cdots, x_{M-1}^{(i)}\right]^T$ in vector notation. The data-modulated symbol sequence is converted by an M-point DFT, $\mathbf{F}_M$, into a frequency domain signal with M components (subcarriers), $\mathbf{s}^{(i)} = \mathbf{F}_M \mathbf{x}^{(i)}$. In the subcarrier mapping part, the symbol vector, $\mathbf{s}^{(i)}$, is mapped into the assigned transmission bandwidth assuming a localized FDMA signal. The operation of the subcarrier mapping is expressed as an N_{FFT} x M matrix, $\mathbf{Q}_{N_{FFT}\times M}$ $(N_{FFT} \ge M)$, where N_{FFT} denotes the number of points for the following inverse FFT (IFFT). In the paper, we set N_{FFT} = 1024. Matrix $\mathbf{Q}_{N_{FFT}\times M}$ is given as $\mathbf{Q}_{N_{FFT}\times M} = \left(\mathbf{0}_{r\times M} \quad \mathbf{I}_M \quad \mathbf{0}_{(N_{FFT}-r-M)\times M}\right)^T$, where r

($r \in \{0,1,...(N_{FFT}-M-1)\}$) represents the subcarrier position in which the 0-th subcarrier of the M-subcarrier signal is assigned and $\mathbf{I}_M$ denotes the M x M unit matrix. After padding (N_{FFT} - M) zeros, the IFFT converts the frequency-domain signal into a time-domain signal as $\mathbf{y}^{(i)} = \mathbf{F}_{N_{FFT}}^{-1}\mathbf{Q}_{N_{FFT}xM}\mathbf{s}^{(i)}$. Here, $\mathbf{F}_{N_{FFT}}^{-1}$ indicates the IFFT matrix. Finally, a CP is appended to each FFT block to avoid inter-block interference.

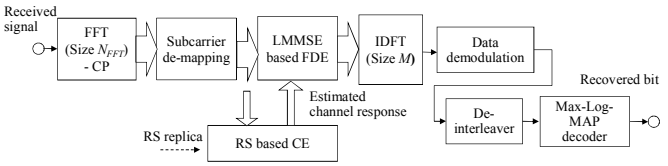

Figure 3. Block diagram of receiver for DFT-precoded OFDMA.

Fig. 3 shows a block diagram of the receiver. At the receiver, one-antenna receiver is assumed, since we focus on the frequency diversity effect. We assume ideal FFT timing detection. After removing the CP, the time domain sample sequence is converted into a frequency domain sample sequence using the FFT. Then, we obtain the desired signals with M subcarriers by removing (N_{FFT} -M) subcarrier components. Let $H(u)$ be the channel response between the transmitter antenna and receiver antenna at each subframe. To reduce the influence of the noise component, we compute a channel estimate at the u-th subcarrier (u = 0, 1, …, M-1), $\hat{H}(u)$, by coherent averaging over $2F_{avg}+1$ subcarriers with the subcarrier of interest as the center as

$$\hat{H}(u) = \sum_{f=-F_{avg}}^{F_{avg}} \alpha_f H(u+f). \quad (4)$$

In (4), coherent summation using weighting factor α_f ($\sum_{f=-F_{avg}}^{F_{avg}} \alpha_f = 1$) is employed. In the evaluation, we set $[\alpha_0, \alpha_{+1/-1}, \alpha_{+2/-2}, \alpha_{+3/-3}, \alpha_{+4/-4}] = [0.2, 0.16, 0.12, 0.08, 0.04]$ for F_{avg} = 4 after optimization based on extensive simulations. The computed $\hat{H}(u)$ is further coherently averaged to $\overline{H}(u)$ over two RS symbols within the duration of a subframe using the channel estimate at each subcarrier after frequency and time domain averaging. The LMMSE weight at the u-th subcarrier is computed as $W(u) = \overline{H}^*(u) \Big/ \left(\left| \overline{H}(u) \right|^2 + \sigma \right)$ [4], where we assume ideal estimation of the noise component, σ, of the LMMSE weight. We compute the squared Euclidian distance between the received symbol after equalization and the symbol replica candidate using the estimated channel impulse response for both bits "0" and "1." We compute the log-likelihood ratio (LLR) of *a posteriori* probability using the minimum squared Euclidean distance for bits "0" and "1." Finally, the LLR is soft-decision turbo decoded using the Max-Log-MAP decoder [16] with eight iterations to recover the transmitted binary data.

IV. Computer Simulation Results

Table I gives the simulation parameters assumed in the paper. The system bandwidth is set to 10 MHz. In localized transmissions, the signal bandwidth is parameterized from B_{Tx} = 2 RBs (= 360 kHz) to 25 RBs (4.5 MHz). In clustered transmissions, the aggregated signal bandwidth is set to B_{Tx} = 12 RBs (= 2.16 MHz). The B_{Tx} is set to 2 RBs for intra-subframe FH. The fading maximum Doppler frequency is set to f_D = 5.55 Hz assuming low mobility such as a pedestrian speed.

A. NFMSV Performance

Fig. 4 shows the computed NFMSV values as a function of the frequency region, f_{reg}, for the four channel models. The figure shows that the 9-path ETU (or 6-path TU) channel model provides a lower NFMSV value compared to that for the 9-path EVA (or 6-path VA) channel model at the same f_{reg} point. This is due to a larger frequency diversity effect caused by the longer delay spread. Moreover, in the TU channel model with the r.m.s. delay spread of approximately 1 μs, the NFMSV value of the 6-path channel becomes smaller than that for the 9-path channel when f_{reg} is narrower than approximately 6 MHz. This is true for the VA channel model, in which the 2 curves for the 9-path and 6-path channels cross at the frequency of approximately f_{reg} = 3 MHz. This is because the small number of paths generates a low correlation with high probability in the narrow frequency region. Meanwhile, in a sufficiently wide frequency region, a greater number of paths generate a lower frequency correlation. Hence, the NFMSV value for the 9-path ETU (or EVA) becomes lower than that for the 6-path TU (or VA) channel model when f_{reg} is greater than approximately 6 (or 3) MHz.

TABLE I. MAJOR RADIO PARAMETERS

Entire transmission bandwidth		10.0 MHz
FFT samples		1024
Transmission bandwidth per UE		2 RBs (360 kHz) - 25RBs (4.5 MHz)
Subcarrier spacing		15 kHz
Symbol duration	Effective symbol duration	66.67 μs
	Cyclic prefix length	4.75 μs
Subframe length		1 ms (14 FFT blocks)
Modulation schemes		QPSK, 16QAM
Channel coding / decoding		Turbo coding (R = 1/3, K = 4 bits) / Max-Log-MAP decoding (8 iterations)
Propagation channel models		• GSM 6-path TU channel model • ITU-R 6-path Vehicular-A channel model • 9-path ETU channel model • 9-path EVA channel model
Number of transmission antennas		N_{Tx} = 1
Number of receiver antennas		N_{Rx} = 1
FFT timing detection		Ideal detection
Equalizer		Frequency domain equalizer (FDE) based on LMMSE criterion
Channel estimation		RS based CE (Ideal CE)

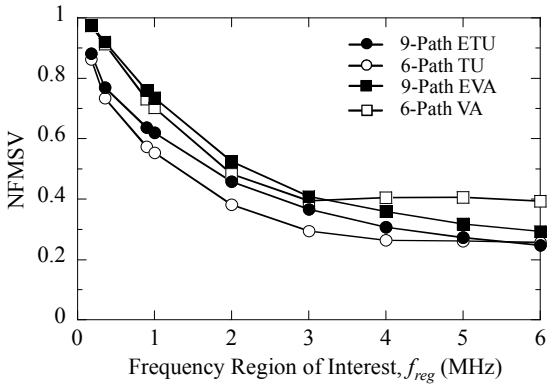

Figure 4. Computed NFMSV as a function of the frequency region of interest, f_{reg}.

B. Average BLER Performance

1) Localized Transmission

Fig. 5 shows the average BLER performance as a function of the average received signal-to-noise power ratio (SNR) for the UE transmission bandwidth of B_{Tx} = 2 RBs (= 360 kHz), 5 RBs (= 900 kHz), and 25 RBs (= 4.5 MHz). In the localized transmission, the B_{Tx} value corresponds to f_{reg}. The six-path TU channel model is assumed. In the figure, the average BLER performance level with RS based channel estimation and that with ideal channel estimation are plotted as solid and dotted lines, respectively. Fig.

5 shows that the average BLER performance level improves according to the increase in the B_{Tx} due to the increasing frequency diversity, i.e., interleaving effect associated with powerful turbo coding. By extending B_{Tx} from 2 RBs to 25 RBs, the required average received SNR at the average BLER of 10^{-2} is decreased by approximately 5.5 dB for the RS based channel estimation. The loss in the required average received SNR for the RS based channel estimation compared to the ideal channel estimation is approximately 0.7 - 1.3 dB.

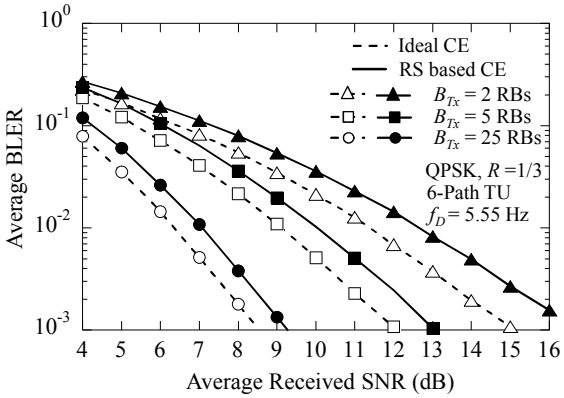

Figure 5. Average BLER performance as a function of the average received SNR for GSM 6-path TU model.

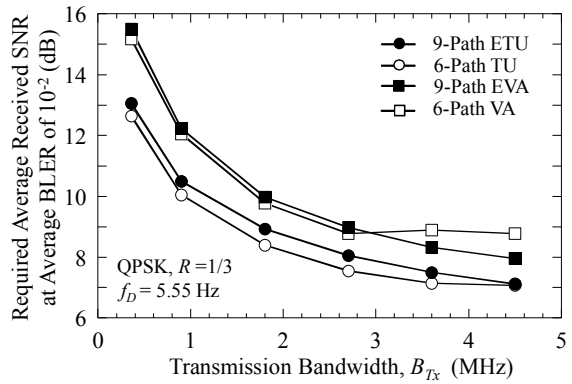

(a) QPSK

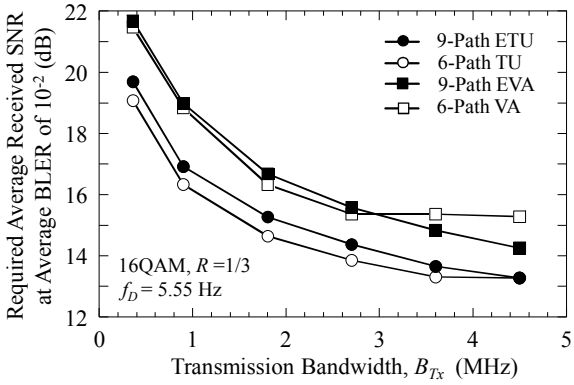

(b) 16QAM

Figure 6. Required average received SNR at average BLER of 10^{-2} for localized transmission as a function of the transmission bandwidth, B_{Tx}.

Focusing on the frequency diversity effect, Figs. 6(a) and 6(b) show the required average received SNR satisfying the average BLER of 10^{-2} as a function of B_{Tx} for QPSK and 16QAM, respectively. Fig. 6(a) shows that the required average received SNR decreases according to the increase in B_{Tx}. Hence, the frequency diversity is very effective in decreasing the required average received SNR according to the increase in the entire frequency region, f_{reg}, in DFT-precoded OFDMA using a FDE. The results mean that frequency diversity is beneficial in randomizing the residual fluctuation in the SINR after employing the FDE. The slopes of the 4 curves well coincide with those of the respective NFMSV curves in Fig. 4. When B_{Tx} is narrower than approximately 4.5 (3.0) MHz for the TU (VA) channel models, the 6-path channel provides a slightly better performance level compared to that for the 9-path channel. In contrast, in a transmission bandwidth wider than the threshold, the 9-path channels provide better performance than the 6-path channels. These results, owing to the frequency diversity, agree well with the NFMSV values in Fig. 4. Fig. 6(b) shows that the required average received SNR increases by approximately 6 dB for 16QAM compared to that for QPSK. However, the same tendencies as those for QPSK are observed for the 4 channel models for 16QAM. Moreover, we confirm that the NFMSV is an accurate measure of the frequency diversity effect in terms of the required average received SNR for DFT-precoded OFDMA using FDE.

2) Clustered Transmission

Fig. 7 shows the average BLER performance levels for clustered transmissions as a function of the average received SNR for the two 9-path channel models. The transmission signal bandwidth is set to B_{Tx} = 12 RBs (= 2.16 MHz). Three types of clustered transmissions are considered: 6 2-RB transmissions with the separation of 4 or 5 RBs each, 3 4-RB transmissions with the separation of 11 RBs each, and 2 6-RB transmissions with the separation of 22 RBs. The corresponding numbers of clusters in the three transmissions are N_c = 6, 3, and 2, respectively, in the entire frequency region of f_{reg} = 34 RBs (= 6.12 MHz). The average BLER performance of the localized transmission with B_{Tx} = 12 RBs is also given as a reference. Fig. 7 shows that average BLER performance level improves distinctly by increasing the number of clusters, N_c, for the ETU channel model. This is due to the increasing frequency diversity effect by multiplexing the transmission signal more dispersedly over the entire transmission bandwidth. We also observe the improvement in the required average received SNR according to the increase in N_c in the EVA channel model. More specifically, the required average received SNR at the average BLER of 10^{-2} for the clustered transmission with N_c = 6 is decreased by approximately 1.5 and 1.8 dB compared to that for the localized transmission in the ETU and EVA channel models, respectively. The decrease in the NFMSV value by extending f_{reg} from 2.16 MHz to 6.12 MHz is almost identical between the ETU and EVA channel models. The relative decrease in the NFMSV corresponds to the relative improvement in the frequency diversity effect in terms of the required average received SNR in both the channel models.

Fig. 8 shows the average received SNR satisfying the average BLER of 10^{-2} as a function of the number of clusters, N_c, in the 9-path ETU and EVA channel models. The performance levels of the 3 signal bandwidths including B_{Tx} = 6 RBs (= 1.08 MHz), 12 RBs, and 18 RBs (= 3.24 MHz) are plotted. For instance, in the case of N_c = 6, 6 1-RB transmissions with the separation of 6 or 4 RBs each and 6 3-RB transmissions with the separation of 3 or 4 RBs each are assumed for B_{Tx} = 6 RBs and 18 RBs, respectively. Fig. 8 shows that according to the increase in the N_c value, the required average received SNR decreases since the transmission signal is multiplexed more dispersedly. However, the

improvement in the required average received SNR is small when N_c is increased beyond approximately 4. Moreover, when the signal bandwidth is wide such as B_{Tx} = 18 RBs, the gain of the clustered transmission becomes small since sufficient frequency diversity is obtained for the localized transmission as confirmed in Fig. 4. In summary, we see that frequency diversity, i.e., the interleaving effect for clustered transmission in terms of the average BLER is well approximated by the relative difference in the NFMSV for the entire frequency region.

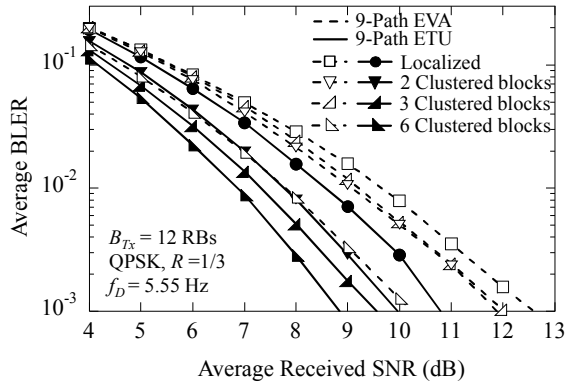

Figure 7. Average BLER performance for clustered transmission in 9-path channel models.

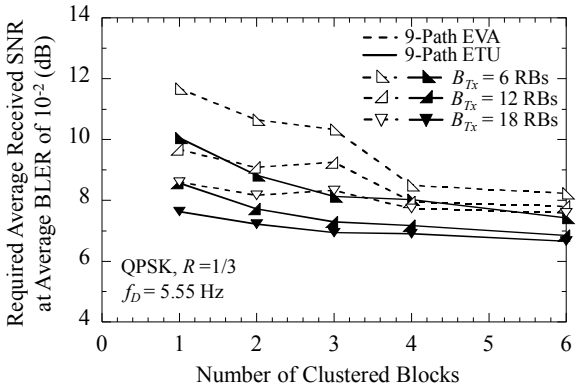

Figure 8. Required average received SNR at average BLER of 10^{-2} for clustered transmission in 9-path channel models.

3) Intra-subframe FH

Fig. 9 shows the required average received SNR at the average BLER of 10^{-2} for intra-subframe FH as a function of the FH separation, f_{FH}. The figure shows that by applying intra-subframe FH with f_{FH} = 2 RBs, the required average received SNR is decreased by greater than approximately 2 and 3 dB compared to that without intra-subframe FH for the ETU (TU) and EVA (VA) channel models, respectively. By extending the FH separation from f_{FH} = 2 RBs to 5 RBs (= 900 kHz), the required average received SNR decreases by approximately 0.5 dB. However, further improvement in the required average received SNR by extending the f_{FH} is slight. Intra-subframe FH is more feasible than FHSS considering the actual CE for coherent detection. However, there is no close relationship between the FH separation and the NFMSV assuming the entire frequency region for the intra-subframe FH, since it does not take advantage of the frequency diversity effect over the entire frequency region.

V. CONCLUSION

This paper presented the frequency diversity effects of localized transmission, clustered transmission, and intra-subframe FH for DFT-precoded OFDMA using a LMMSE based FDE. In the evaluations, we employ the NFMSV as a measure of the frequency diversity effect, i.e., frequency domain interleaving effect associated with turbo coding. Link-level computer simulation results showed that frequency diversity is very effective in decreasing the required average received SNR at the target average BLER according to the increase in the entire frequency region, f_{reg}, in the DFT-precoded OFDMA using FDE. The results indicate that frequency diversity is beneficial in randomizing the residual fluctuation in the SINR after employing a FDE. Moreover, we showed that the NFMSV is an accurate measure of the frequency diversity effect for localized transmission in terms of the average BLER, and that the NFMSV for the entire frequency region, f_{reg}, approximates well the frequency diversity effect for clustered transmission. Finally, we showed that the effect of intra-subframe FH is saturated at the FH separation of approximately 5 RBs (= 900 kHz) for the ETU and ETA channel models, and that there is no close relationship between the FH separation and the NFMSV assuming the entire frequency region for the intra-subframe FH.

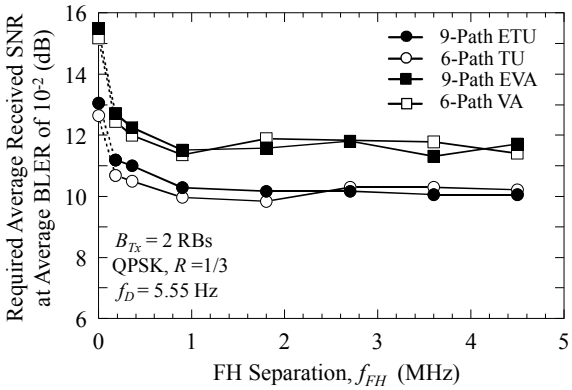

Figure 9. Required average received SNR at average BLER of 10^{-2} as a function of FH separation, f_{FH}.

REFERENCES

[1] 3GPP TS36.211 (V8.9.0), Dec. 2009.
[2] D. Galda and H. Rohling, Proc. of IEEE VTC2002-Spring, vol. 4, May 2002.
[3] R. Dinis, *et al.*, Proc. of IEEE Globecom, vol. 6, Dec. 2004.
[4] H. Sari, *et al.*, Proc. of IEEE IEEE Globecom, vol. 1, Nov.–Dec. 1994.
[5] D. Falconer, *et al.*, IEEE Commun., Mag., vol. 40, Apr. 2002.
[6] 3GPP TS36.211 (V10.3.0), Sept. 2011.
[7] J.G. Proakis, *Digital Communications*, McGraw-Hill International Edition, 2001.
[8] A. Goldswith, *Wireless Communications*, Cambridge University Press, 2005.
[9] J.C. Liberti, Jr. and T.S. Rappaport, *Smart Antennas for Wireless Communications*, Prentice Hall, 1999.
[10] D.-S. Yoo, *et al.*, Proc. of IEEE VTC2000-Spring, May 2000.
[11] D.-S. Yoo and W.E. Stark, IEEE Trans. on Wireless Commun., vol. 4, no. 4, pp. 1575-1484, July 2005.
[12] 3GPP TS 45.005 (V9.4.0), Sept. 2010.
[13] "Guidelines for evaluation of radio transmission technologies for IMT-2000," Recommendation ITU-R M.1225, 1997.
[14] 3GPP TS 36.104 (V10.0.0), Sept. 2010.
[15] 3GPP TS36.212 (V8.8.0), Dec. 2009.
[16] P. Robertson, *et al.*, of Proc. IEEE ICC'95, vol. 2, pp. 1009-1013, June 1995.